Liquid-liquid phase separation and amyloid aggregation in the 14-3-3 protein family

Viktorija Karalkevičiūtė[1†], Saulė Rapalytė[1†], Ieva Baronaitė[1,2], Dominykas Veiveris[1], Vytautas Smirnovas[1], Mantas Žiaunys[1], Darius Šulskis[1*]

[1]Institute of Biotechnology, Life Sciences Center, Vilnius University, Vilnius, Lithuania

[2]Current address: Centre for Misfolding Diseases, Yusuf Hamied Department of Chemistry, University of Cambridge, Lensfield Road, Cambridge CB2 1EW, United Kingdom

[†]These authors contributed equally to this work.

*Correspondence should be addressed to
Email: darius.sulskis@gmc.vu.lt

Abstract:

The 14-3-3 protein family, with over 1300 binding partners, is one of the largest regulators of protein-protein interactions (PPIs) in eukaryotic cells. They recognise and bind to phosphorylation-related motifs in their partner proteins, creating scaffolds to stabilise proteins and allowing or inhibiting kinases' access to their targets. 14-3-3 consists of seven isoforms (β, γ, ε, ζ, η, θ and σ), which are expressed across all tissues.

Given their important role in PPIs, their dysregulation can contribute to a variety of diseases, such as cancer or neurodegenerative disorders like Creutzfeldt-Jakob's, Parkinson's or Alzheimer's diseases. Pathological effects can arise due to loss of function, aberrant interactions or protein aggregation. Notably, 14-3-3 aggregates have been detected in Lewy bodies or cerebrospinal fluid, mirroring the presence of amyloid proteins, such as α-synuclein or β-amyloid. Toxic amyloid aggregation signals the onset of neurodegeneration, which can occur through misfolding of proteins or liquid-liquid phase separation (LLPS) – a process during which proteins condense into membraneless organelles.

Unlike other amyloidogenic proteins, there is little information on the conditions under which the 14-3-3 protein family members undergo LLPS or their relationship with amyloid aggregation. To address this gap, we examined all isoforms of 14-3-3 *in vitro* and observed the formation of amyloid aggregates and phase-separated droplets. Our results revealed that the ε and θ isoforms form worm-like fibrils, and molecular crowding conditions promote phase separation in most of the 14-3-3 proteins.

Introduction

The 14-3-3 protein family is one of the key interaction hubs that coordinate protein-protein interactions (PPIs) in mammals and plants [1]. They can create scaffolds that facilitate protein binding with their partners, or they can block and dissociate complexes. Most commonly, 14-3-3s recognise phosphorylation motifs and help kinases or phosphatases reach their targets [2]. 14-3-3 isoforms are evolutionarily conserved [1] and expressed in most tissues, but especially in the brain, where they can comprise up to 1% of soluble proteins [2]. Thus, they also interact with numerous neurodegeneration-linked proteins such as tau [3], α-synuclein [4] and coordinate their PPIs [5].

A key pathological feature of tau and α-synuclein is that they form insoluble protein aggregates known as amyloids [6], which are considered to be the central hallmarks of Alzheimer's and Parkinson's diseases, respectively [7], [8]. Amyloid plaques often contain not only these proteins, but also their interaction partners that co-aggregate together due to spatial proximity and affinity [9]. One of the early steps that promotes protein aggregation is liquid-liquid phase separation (LLPS), during which proteins condense into membraneless droplets, resulting in a local increase in protein concentration. LLPS can facilitate interactions between proteins, DNA, and RNA [10], [11], [12], and also accelerate the aggregation of proteins due to a crowded environment [13].

14-3-3s are found in Lewy bodies due to co-interactions with α-synuclein [14] and can mitigate α-synuclein aggregation [4] as well as reduce the propagation of amyloid fibrils [15]. Notably, a recent study showed that potential 14-3-3 amyloid structures also exist in tumor-derived cell lines [16]. Beyond amyloidogenesis, 14-3-3s have been suggested as potential regulators of LLPS. Among 1370 analysed binding partners, roughly half of them had a high propensity for phase separation [17]. Some examples include the microtubule-binding protein tau, where 14-3-3ζ prevents both aggregation and condensation of phosphorylated tau [18]. 14-3-3s also stabilise tumour suppressor factor p53 [19] and bind to SARS-CoV-2 nucleocapsid protein in low micromolar concentrations [20]. Both p53 [21] and nucleocapsid [22] are phase-separating proteins with critical roles in cancer or SARS-CoV-2 replication. Despite these numerous interactions with LLPS-forming proteins, it remains unknown whether 14-3-3 proteins themselves are capable of undergoing phase separation and forming amyloid fibrils.

Recently, our laboratory showed that 14-3-3ζ can form short amyloid fibrils [23]; interestingly, other isoforms share conserved sequence features that may predispose them to similar behaviour [24]. In this study, we systematically investigate the amyloidogenic and LLPS propensities of all seven 14-3-3 isoforms *in vitro*. We combined computational predictions of aggregation-prone regions and LLPS-associated domains with experimental analyses of protein stability, aggregation, and phase separation. Our main results revealed that most 14-3-3 proteins undergo phase separation

under *in vitro* molecular crowding conditions, and that the ε isoform is the most amyloidogenic, forming characteristic worm-like fibrils.

Methodology

Multiple Sequence Alignment

Sequences of *Homo sapiens* 14-3-3 isoforms (β, γ, ε, ζ, η, θ and σ) were obtained from the Uniprot database [25]. Sequences were aligned using MUSCLE (Multiple Sequence Comparison by Log-Expectation) [26] with default parameters and edited via Jalview [27].

Cloning

The 6xHis-SUMO-14-3-3 β, γ, ε, η, and θ constructs were derived from pGEX-2TKGST-14-3-3 (Addgene no. 13276, 13280, 13279, 13277, 13281) [2]. The 14-3-3 genes and the SUMO-tag were amplified and fused using standard PCR methods. The products were inserted into a pET28b(−) vector via NdeI and XbaI restriction sites by standard cloning techniques, yielding 14-3-3s constructs fused to an amino-terminal 6xHis-SUMO tag.

pGEX-2TK-14-3-3 beta, gamma, epsilon, eta, tau GST were gifts from Michael Yaffe (Addgene plasmid # 13276, 13280, 13279, 13277, 13281; http://n2t.net/addgene:13276/13280/13279/13277/13281; RRID:Addgene_13276/13280/13279/13277/13281). pET28-6xHix-14-3-3ζ and σ were gifts from Prof. B.M. Burmann. The plasmids and primers used in this study are listed in Table S1.

Protein Expression and Purification

The purification of 14-3-3 isoforms was done as previously described [23] with minor modifications. In short, plasmid constructs encoding 6xHis-SUMO-tagged 14-3-3 isoforms (β, γ, ε, ζ, η, θ or σ) were transformed into One Shot BL21 Star (DE3) *Escherichia coli* (Thermo Scientific) cells by heat shock at 42 °C for 45 s. Transformed cells were grown in 100 mL of LB medium containing kanamycin (50 µg/mL) at 37 °C and 220 rpm for 16 h. The culture was transferred to 300 mL ZYM-5052 autoinduction medium [28] with kanamycin (50 µg/mL) and incubated at 30 °C and 220 rpm for 16 h. Cells were harvested by centrifugation (3000 g, 20 min, 4 °C). The biomass was resuspended in a buffer (50 mM HEPES and 1.0 M NaCl, pH 7.5), followed by the addition of lysozyme (0.2 mg/ml) and 1 mM phenylmethylsulfonyl fluoride (PMSF). Cells were lysed by sonication (Sonopuls, VS70T probe; Bandelin) for 30 min at 40% amplitude, with a 15 s on/30 s off cycle. The lysate was centrifuged (18 000 g, 30 min, 4 °C). The supernatant was then filtered through a 0.45 µm pore size filter and applied to a gravity column packed with Ni^{2+} Sepharose 6 Fast Flow resin (Cytiva). The column was washed with 50 mM HEPES and 1.0 M NaCl (pH 7.5) buffer, followed by elution with the same buffer solutions containing 0.05 and 0.5 M imidazole. Fractions containing 6xHis-SUMO-tagged 14-3-3 protein were dialyzed (8000 Da MWCO,

Biodesign D106) against a 10 mM potassium phosphate buffer (pH 8.0) for 1 h. Home-made Sentrin-specific protease 1 domain (SENP1) was added to cleave the 6xHis-SUMO tag, and the samples were dialyzed for an additional 18 h against a fresh 10 mM potassium phosphate buffer (pH 8.0). Then, the samples were centrifuged (3160 g, 30 min, 4 °C) and filtered through a 0.45 µm pore size filter. Purification using a gravity column was repeated to collect the flow-through fractions. All fractions were checked by SDS-PAGE. Before size exclusion chromatography, 10 mM EDTA and 10 mM dithiothreitol (DTT) were added to all samples. The samples were then concentrated (10 kDa MWCO, Merck) and filtered through a 0.22 µm pore size filter. Size exclusion chromatography was performed using a Tricorn 10/300 (Cytiva) column packed with Superdex 75 resin (Cytiva) and calibrated with PBS (pH 7.4) buffer. The collected fractions were checked by SDS-PAGE and concentrated (10 kDa MWCO, Merck). The protein samples were stored at −80 °C.

Aggregation kinetics and liquid-liquid phase separation

Samples for the aggregation kinetics assay were prepared by mixing 100 µM of each purified 14-3-3 isoform in PBS buffer (pH 7.4) with 50 µM amyloid-specific Thioflavin-T (ThT) dye. Each sample was divided into four wells of a 96-well non-binding plate, with each well containing a 3 mm glass bead (Merck, cat. No 1040150500). Aggregation kinetics were measured every 10 min at 37 °C with constant shaking at 600 rpm between the measurements using a CLARIOstar Plus microplate reader. ThT dye was excited at 440 nm, and the emission signal was recorded at 480 nm.

For LLPS studies, samples were prepared identically as for aggregation kinetics, but with the addition of 10% or 20% of the crowding agent polyethylene glycol solution (PEG, 20 kDa, Thermo Scientific), without the 3-mm glass bead and constant shaking. ThT fluorescence and optical density at 600 nm (OD_{600}) were measured every 10 minutes at 37 °C.

Atomic Force Microscopy (AFM)

The freshly cleaved mica was positively charged by applying 50 µL of 0.5% (3-aminopropyl)triethoxysilane (APTES) on the surface and allowing it to functionalize for 5 min. Subsequently, the mica was washed with dH_2O and dried with airflow, and the procedure was repeated with 50 µL of the protein sample, which was prepared by diluting it 1:9 with PBS buffer. Imaging was performed using a Dimension Icon microscope (Bruker) operating in tapping-in-air mode with aluminium-coated silicon tips (RTESPA-300, Bruker). The images were processed using Gwyddion 2.66 software [26].

Fourier Transform Infrared (FTIR) Spectroscopy

Each purified 14-3-3 isoform was diluted to 100 μM in PBS buffer (pH 7.4) and distributed to 1.5 mL test tubes (400 μL final volume, each test tube contained two 3 mm glass beads (Merck, cat. No 1040150500)). The samples were incubated at 37 °C with constant agitation at 600 rpm agitation for 67 h.

The aggregated samples were centrifuged at 16 900 g for 30 min, after which the supernatant was removed and replaced with 400 μL of D_2O supplemented with 500 mM NaCl (the addition of NaCl generally improves fibril sedimentation) [29]. The centrifugation and resuspension procedures were repeated four times. After the final step, the aggregate pellet was resuspended in 50 μL of D_2O containing 500 mM NaCl.

FTIR spectra were acquired as described previously [30] using an Invenio S FTIR spectrometer (Bruker), equipped with a liquid nitrogen-cooled mercury-cadmium-telluride detector, at room temperature with constant dry-air purging. For each sample, 256 interferograms with 2 cm^{-1} resolution were recorded and averaged. D_2O containing 400 mM NaCl and water vapor spectra were subtracted from each sample spectrum, followed by baseline correction and normalization to the same 1595–1700 cm^{-1} wavenumber range. All data processing was performed using GRAMS software.

Far-UV Circular Dichroism (CD) Spectroscopy

Protein aggregation was performed by incubating samples in 1.5 mL microcentrifuge tubes (Eppendorf) with a 3 mm glass bead at 37 °C for 67 hours with constant agitation at 600 rpm. The samples were then placed in a 0.5 mm quartz cuvette, and CD spectra were measured using a J-815 spectropolarimeter (Jasco). For each sample, spectra were recorded between 190 and 260 nm at 0.1 nm intervals. The data was smoothed using a Savitzky-Golay filter with a 3 nm window. Data analysis was performed using ChiraKit software [27].

Differential Scanning Fluorimetry (DSF)

Samples for the protein stability assay were prepared by mixing 100 μM of each 14-3-3 isoform in PBS buffer (pH 7.4) with 100 μM 8-anilinonaphthalene-1-sulfonic acid (ANS). The ANS concentration was determined using its extinction coefficient ($\varepsilon_{351\ nm}$ = 5500 M^{-1} cm^{-1}). Protein unfolding was monitored with a Rotor-Gene Q instrument (QIAGEN) using the blue channel (excitation, 365 ± 20 nm; detection, 460 ± 20 nm). The unfolding process was initiated by ramping the temperature from 25 to 99 °C at 1 °C/min increments. Data analysis was performed using MoltenProt software [28].

Fluorescence Microscopy

14-3-3 isoforms were labelled with fluorescein isothiocyanate (FITC) as described previously [31]. The samples for fluorescence microscopy were prepared by mixing 1 μM FITC-labelled 14-3-3 isoform with 99 μM unlabeled isoform in PBS buffer (pH 7.4). PEG (20 kDa) was added to reach final concentrations of 10% and 20%. Each sample was measured immediately after mixing (0 h) and again after 1 h.

15 μL aliquots of each sample were pipetted onto 1 mm glass slides (Fisher Scientific, cat. No. 11572203), covered with 0.18 mm coverslips (Fisher Scientific, cat. No. 17244914) and imaged immediately after preparation. Short movies were acquired using Olympus IX83 microscope with a 40x objective and fluorescence filter cubes (480 nm excitation and 530 nm emission). Four different images were cropped from each movie and analyzed using Fiji software [32]. Full movies and additional fluorescence microscopy images are available in an online data repository at: doi: 10.5281/zenodo.17709463

Droplet statistical analysis

To determine the size of droplets, four fluorescence microscopy images of each 14-3-3 isoform were analyzed. Droplets were segmented using color-based thresholding in ImageJ [29] software, followed by particle analysis. Circular particles (circularity value = 1.0) with a minimum of four pixels in size were included in the droplet area analysis.

Results

Amyloid and Phase-Separation Potential of 14-3-3

Interpretation of amyloidogenic and LLPS properties of 14-3-3 proteins is still at an early stage, indicating a gap in characterising their potential function or disease-related impact. To address this, we initially checked for amyloidogenic regions of 14-3-3 proteins using WALTZ [24] and LLPS propensities with PSPHunter web servers [25]. The WALTZ algorithm identified that all members have aggregation-prone regions between 170 and 185 amino acids (Fig. 1A), specifically within the sixth α-helix of the proteins. Three members (β, ε, ζ) had an additional 145-153 amino acid region (fifth α-helix), suggesting a structurally inherent susceptibility to misfolding or aggregation. Conversely, all proteins were given low-probability scores (Fig. S1) for LLPS propensities, with 14-3-3ε and 14-3-3ζ having the highest scores (0.4 and 0.37, respectively). The LLPS sequences between different family members were spread (Fig. S2), but most showed the N-terminal as the most likely droplet-forming region. Alignment of 14-3-3 sequences (Fig. S2) indicated no overlapping aggregation-prone or LLPS regions; however, a high consensus of previously identified 170-185 aggregation-prone region was observed between isoforms.

To supplement the sequence-based aggregation and LLPS propensity, we measured their melting temperature using differential scanning fluorimetry (DSF) to assess their global stability. Between different 14-3-3 members, the unfolding temperature (T_m) ranged from 53°C to 64°C, with the least stable member being 14-3-3η (53.5 ± 0.1°C) and the most stable - 14-3-3σ (63.5 ± 0.1°C). The results closely matched those of previously reported T_m values of β, γ, ε, θ, and σ isoforms [33]. The unfolding temperatures of all proteins varied by less than 10°C, indicating similar stability of all isoforms. Overall, 14-3-3 proteins contain aggregation-prone regions but display low score LLPS propensity and generally are stable proteins. However, due to the limited experimental data available on their amyloid aggregation and phase-separation behaviour, current predictions are highly limited and prone to error. Hence, we further investigated each propensity experimentally.

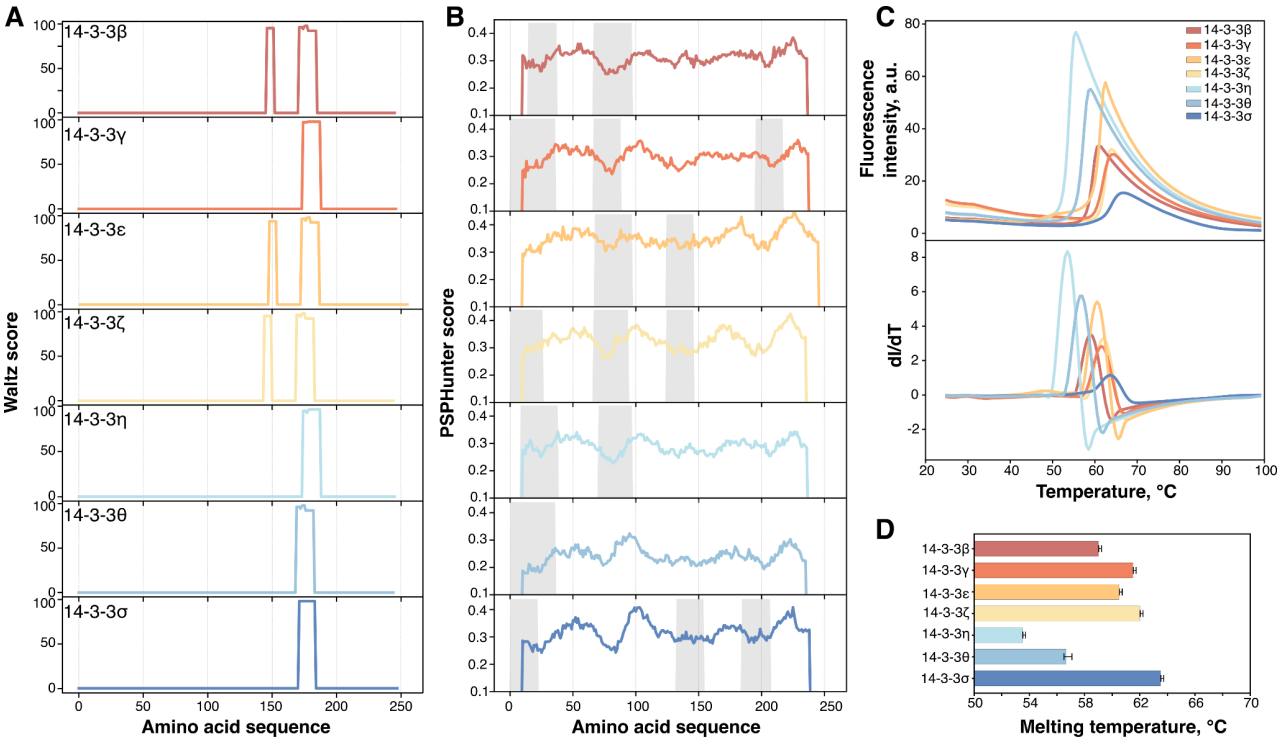

*Figure 1. (**A**) Amyloidogenic regions of 14-3-3 isoforms predicted by the WALTZ* [34] *web server. (**B**) Prediction of LLPS-driving regions by PSPHunter* [35]*, grey areas indicate the most probable phase-separating sequences. (**C**) Melting curves, including the first derivatives profiles, of 14-3-3 isoforms and (**D**) calculated melting temperatures by MoltenProt* [36].

Amyloid aggregation of 14-3-3 protein

We investigated aggregation properties of each protein using the amyloid specific dye Thioflavin T (ThT) [37], whose fluorescence intensity increases upon binding to fibrils. Aggregation kinetics were monitored over 42 hours at 37 °C, and only the 14-3-3ε sample displayed increased ThT fluorescence, indicating amyloid formation (Fig. 2A).

Next, we assessed the secondary structure of each isoform before and after 42 h incubation using circular dichroism (CD) (Fig. 2B). As expected, all proteins natively contained α-helices, and after the incubation, the ellipticity increased compared to native spectra, indicating changes in secondary structure or heterogeneity between soluble protein and aggregates. Only 14-3-3γ spectra did not exhibit any changes, which suggests the inherent high stability of the protein. To determine if aggregates have β-sheet structures, we isolated them by centrifugation and recorded Fourier transform infrared (FTIR) spectra. β, ε, η, γ isoforms had a sufficient amount of aggregates for detection, and all spectra exhibited a characteristic 1618-1620 nm^{-1} peak (Fig. S3) [38], which indicates the formation of β-sheets. 14-3-3 ζ, θ, σ aggregates were too small or insufficient to pellet at this stage of aggregation, though β-sheet structures in ζ have previously been detected after a

longer incubation [23], which was not performed here due to ThT dye bleaching in constant fluorescence measurements [39].

Finally, atomic force microscopy (AFM) imaging of each sample showed that most members form unspecific shape aggregates or oligomers, whereas 14-3-3ε produced worm-like fibrils with an average height of 1.83 nm (Fig. S4), similar to those previously observed in S100A9 [40], prion protein [41] and TDP43 nucleic acid binding domain [42]. Fibrils were also observed in a 14-3-3θ sample, but in a lower quantity.

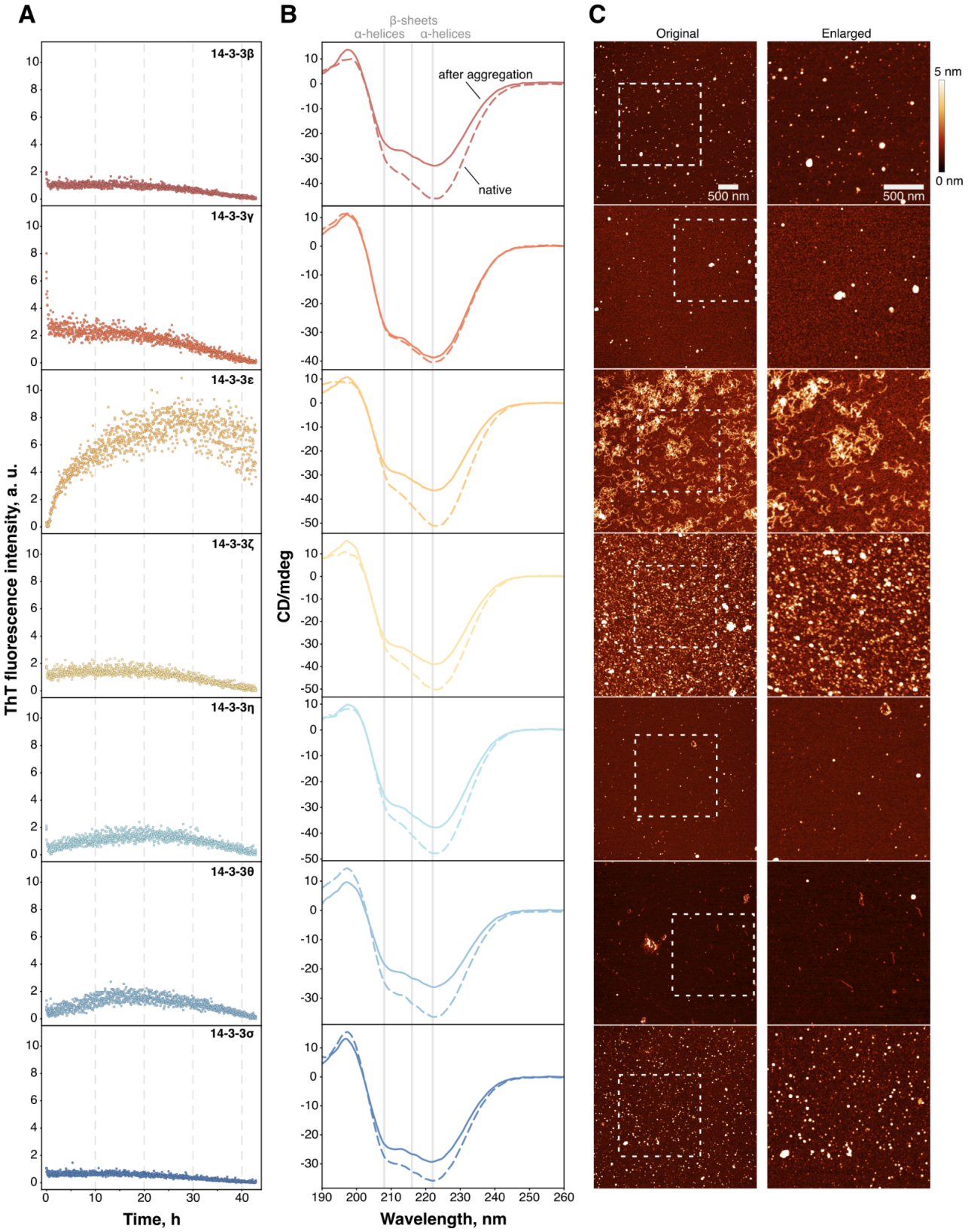

*Figure 2. (**A**) Aggregation kinetics of 14-3-3 proteins as observed by ThT fluorescence (**B**). CD spectra of 14-3-3 proteins after aggregation. All samples were incubated for 42 h at 37 ℃. The dashed line indicates the native protein spectra, while the solid line represents the spectra after aggregation. (**C**) AFM images of 14-3-3 aggregates (scale bar = 500 nm). The square with dashed lines shows an enlarged part of the image.*

LLPS of 14-3-3 proteins

Amyloid aggregation and LLPS often are intertwined processes. The high local concentration of proteins within phase-separated droplets can promote their aggregation [43] and, in some cases, is linked to the initiation of amyloid formation [13]. Currently, there are no data regarding 14-3-3 LLPS behaviour, therefore, we decided to screen them using LLPS-inducing conditions in the presence of PEG.

14-3-3 proteins were labelled with a green fluorescent dye (FITC) and mixed with non-labelled protein in a ratio of 1 to 99, to avoid the influence of FITC modification [31], [44]. The samples for fluorescence microscope imaging were taken immediately and after 1 hour of incubation at room temperature. In the control sample without PEG (Fig. S5), unspecific aggregates or small and isolated droplets were observed. However, at 10% PEG (Fig. S6A) and 20% PEG (Fig. 2A), more evident LLPS and aggregation were observed. The largest condensates were noticed in β, γ, η and θ isoforms, however, across all measured samples, small-sized droplets/aggregates predominated, with a median area ranging from 0.65 to 1.53 μm^2 (Fig. S7).

To further characterise the process, we also monitored the kinetics of LLPS via turbidity of the solution and ThT fluorescence over 67 h at 37 °C. For most 14-3-3 isoforms, 67 h was insufficient for the signal to reach a plateau, confirming that the transition from LLPS to aggregation of 14-3-3 proteins is a slow process, similar to non-LLPS conditions (Fig. 3B). Only 14-3-3ε aggregation was completed within this period, which coincides with amyloid aggregation. In the presence of 10% PEG, kinetics were also slow, with lower ThT fluorescence intensities (Fig. S6B). Comparison of endpoint values revealed that 14-3-3θ and 14-3-3ε had the highest ThT fluorescence levels, as well as an elevated (>0.5 O.D.) turbidity, suggesting the formation of larger droplets or aggregation. 14-3-3η initially showed a high OD jump, but decreased during incubation, which corresponds to dissolution of initial aggregates observed in fluorescence microscope images. In comparison to 20 % PEG conditions, at 10% of PEG, 14-3-3ε exhibited the highest ThT fluorescence, while 14-3-3θ ThT fluorescence was comparable to other isoforms, (Fig. S6C). Furthermore, turbidity was uniformly lower (<0.5 O.D) across all samples.

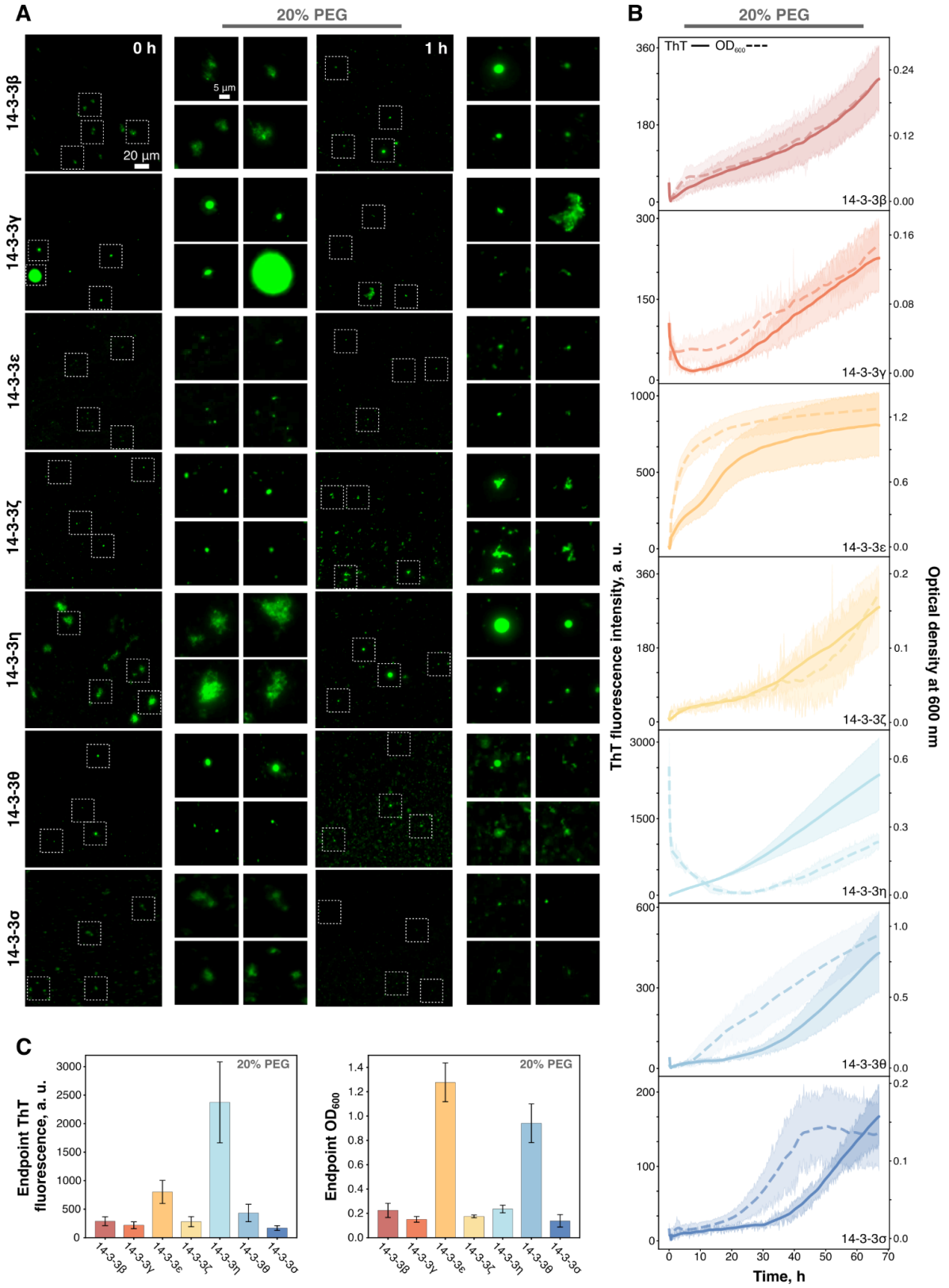

*Figure 3. (**A**) Fluorescence microscopy images of 14-3-3 droplets and aggregates formed initially (0 h) and after 1 h (scale bar = 20 µm). Squares with dashed lines indicate enlarged parts of the images (scale bar = 5 µm). (**B**) LLPS kinetics of 14-3-3 proteins in the presence of 20% PEG, followed by ThT fluorescence (solid line) and optical density (dashed line) for 67 h at 37 ℃. (**C**) Endpoint ThT intensities and OD values of LLPS measurements.*

Discussion

The most important function of the 14-3-3 family is acting as a scaffold for various protein interactions. In the cellular environment, interactions between protein-protein or protein-nucleic acids (DNA/RNA) can occur through LLPS, especially in cases with non-globular proteins or proteins found in the nucleus and RNP granules [45]. 14-3-3 can modulate such phase-separated interactions. For example, phosphorylated tau protein undergoes phase separation, but binding to 14-3-3 inhibits LLPS and amyloid aggregation [18]. 14-3-3ζ can also be incorporated within Tau droplets and stabilise them, but impede Tau droplet-driven tubulin assembly [46]. Similarly, condensates of the human RNA-binding protein SMAUG1 are dissolved by 14-3-3γ or ζ by the co-expression in cells [47]. Another example is LRRK2 kinase, which phosphorylates α-synuclein, but becomes inactivated upon forming a 14-3-3 complex [5]. Finally, one of the most promoting phase-separating environments in a cell is in the nucleus [48], and 14-3-3 isoforms can be located there. The isoform forming the largest droplets, 14-3-3β, is predominantly localized in neuronal nuclei, whereas 14-3-3γ is found in astrocytic nuclei and 14-3-3ζ in the nuclei of oligodendrocytes [49]. Furthermore, 14-3-3s contain nuclear export signal (NES), which enables them to shuttle other proteins from the nucleus [50], however underlying mechanisms are still not fully understood. With hundreds of known phase-separating partners, it remains unclear how the LLPS of 14-3-3 proteins themselves may influence their binding interactions, as potentially it could create hubs for more efficient binding or prevent unwanted reactions.

Protein aggregation is closely associated with neurodegeneration, both because amyloids can be intrinsically toxic and because aggregation leads to loss of protein function. Recently, elevated levels of 14-3-3γ, β and ζ in cerebrospinal fluid (CSF) have been strongly associated with cognitive decline in early AD. Notably, the γ isoform appears to be more prevalent than classical CSF AD biomarkers [51]. Furthermore, loss of the 14-3-3ε gene is associated with increased anxiety, memory dysfunction [52], critical for preventing lissencephaly [53]. Thus, aggregation of 14-3-3ε could potentially contribute to similar dysfunctions. 14-3-3 isoforms ε, θ have already been shown to co-localise with ALS linked SOD1 aggregates [54] and ε is a component of prion protein amyloid deposits of Gerstmann-Sträussler-Scheinker disease (GSS) [55]. 14-3-3 isoforms can also recruit proteins in the aggresome formation pathway [56], resolubilize aggregates [57] and act as moonlight chaperones [58]. All these studies support the hypothesis that 14-3-3 aggregation may influence, or be influenced by, the aggregation of other proteins.

Conclusions

Overall, these results add 14-3-3 to the growing list of proteins that can undergo LLPS and form

amyloid fibrils *in vitro*. Although many studies have reported their co-localization with aggregates, our work directly demonstrates that 14-3-3 proteins themselves can phase separate and aggregate. A limitation of the current study is that we did not investigate these properties *in vivo*; however given that dysregulated condensate dynamics and protein aggregation are increasingly implicated in neurodegeneration, understanding how 14-3-3 transitions between soluble, condensed, and aggregated states may provide new insights into disease pathogenesis and identify potential therapeutic targets.

Acknowledgements: We would like to thank Michael Yaffe and Björn M. Burmann for providing the plasmids used in this study.

Funding: No external funding was received for this study.

Author Contribution:

Viktorija Karalkevičiūtė - Formal Analysis, Investigation, Methodology, Writing - Original Draft, Writing -Review & Editing, Visualization. **Saulė Rapalytė: -** Formal Analysis, Investigation, Methodology, Writing - Original Draft, Writing -Review & Editing, Visualization. **Ieva Baronaitė**: Formal Analysis, Investigation, Methodology, Writing - Original Draft, Writing -Review & Editing, **Dominykas Veiveris:** Methodology, **Mantas Žiaunys:** Methodology, Writing -Review & Editing **Vytautas Smirnovas**: Resources, Writing -Review & Editing. **Darius Šulskis**: Conceptualization, Formal Analysis, Investigation, Methodology, Writing - Original Draft, Writing -Review & Editing, Visualization.

Competing interests:

The authors declare that they have no competing interests.

Data and materials availability:

All data needed to evaluate the conclusions in the paper are present in the paper and/or Supplementary Materials. The raw data used in this paper have been archived and are available on Zenodo: 10.5281/zenodo.17709463. All other relevant data are available from the corresponding author upon reasonable request.

References

[1] X. Yang *et al.*, ‘Structural basis for protein–protein interactions in the 14-3-3 protein family’, *Proc. Natl. Acad. Sci. U.S.A.*, vol. 103, no. 46, pp. 17237–17242, Nov. 2006, doi: 10.1073/pnas.0605779103.

[2] M. B. Yaffe *et al.*, ‘The Structural Basis for 14-3-3:Phosphopeptide Binding Specificity’, *Cell*, vol. 91, no. 7, pp. 961–971, Dec. 1997, doi: 10.1016/S0092-8674(00)80487-0.

[3] Y. Chen *et al.*, ‘14-3-3/Tau Interaction and Tau Amyloidogenesis’, *Journal of Molecular Neuroscience*, vol. 68, no. 4, pp. 620–630, 2019, doi: 10.1007/s12031-019-01325-9.

[4] R. Underwood *et al.*, ‘14-3-3 mitigates alpha-synuclein aggregation and toxicity in the in vivo preformed fibril model’, *acta neuropathol commun*, vol. 9, no. 1, p. 13, Dec. 2021, doi: 10.1186/s40478-020-01110-5.

[5] J. A. Martinez Fiesco *et al.*, ‘14-3-3 binding maintains the Parkinson’s associated kinase LRRK2 in an inactive state’, *Nat Commun*, vol. 16, no. 1, p. 7226, Aug. 2025, doi: 10.1038/s41467-025-62337-1.

[6] A. A. Nizhnikov, K. S. Antonets, and S. G. Inge-Vechtomov, ‘Amyloids: from Pathogenesis to Function.’, *Biochemistry. Biokhimiia*, vol. 80, no. 9, pp. 1127–44, 2015, doi: 10.1134/S0006297915090047.

[7] H. Hampel *et al.*, ‘The Amyloid-β Pathway in Alzheimer’s Disease’, *Mol Psychiatry*, vol. 26, no. 10, pp. 5481–5503, Oct. 2021, doi: 10.1038/s41380-021-01249-0.

[8] A. Recasens and B. Dehay, ‘Alpha-synuclein spreading in Parkinson’s disease’, *Front. Neuroanat.*, vol. 8, Dec. 2014, doi: 10.3389/fnana.2014.00159.

[9] H. Olzscha *et al.*, ‘Amyloid-like Aggregates Sequester Numerous Metastable Proteins with Essential Cellular Functions’, *Cell*, vol. 144, no. 1, pp. 67–78, Jan. 2011, doi: 10.1016/j.cell.2010.11.050.

[10] S. Chakraborty *et al.*, ‘Liquid-liquid phase separation in subcellular assemblages and signaling pathways: Chromatin modifications induced gene regulation for cellular physiology and functions including carcinogenesis’, *Biochimie*, vol. 223, pp. 74–97, Aug. 2024, doi: 10.1016/j.biochi.2024.05.007.

[11] D. W. Sanders *et al.*, ‘Competing Protein-RNA Interaction Networks Control Multiphase Intracellular Organization’, *Cell*, vol. 181, no. 2, pp. 306-324.e28, Apr. 2020, doi: 10.1016/j.cell.2020.03.050.

[12] J. Gu *et al.*, ‘Hsp40 proteins phase separate to chaperone the assembly and maintenance of membraneless organelles’, *Proc. Natl. Acad. Sci. U.S.A.*, vol. 117, no. 49, pp. 31123–31133, Dec. 2020, doi: 10.1073/pnas.2002437117.

[13] S. Mukherjee, M. Poudyal, K. Dave, P. Kadu, and S. K. Maji, ‘Protein misfolding and amyloid nucleation through liquid–liquid phase separation’, *Chem. Soc. Rev.*, vol. 53, no. 10, pp. 4976–5013, 2024, doi: 10.1039/D3CS01065A.

[14] Y. Kawamoto, I. Akiguchi, S. Nakamura, Y. Honjyo, H. Shibasaki, and H. Budka, ‘14-3-3 Proteins in Lewy Bodies in Parkinson Disease and Diffuse Lewy Body Disease Brains’, *J Neuropathol Exp Neurol*, vol. 61, no. 3, pp. 245–253, Mar. 2002, doi: 10.1093/jnen/61.3.245.

[15] B. Wang *et al.*, ‘14-3-3 Proteins Reduce Cell-to-Cell Transfer and Propagation of Pathogenic α-Synuclein’, *J. Neurosci.*, vol. 38, no. 38, pp. 8211–8232, Sept. 2018, doi: 10.1523/JNEUROSCI.1134-18.2018.

[16] D. Alem *et al.*, ‘Amyloids in bladder cancer hijack cancer-related proteins and are positive correlated to tumor stage’, *Sci Rep*, vol. 15, no. 1, p. 4393, Feb. 2025, doi: 10.1038/s41598-025-88307-7.

[17] X. Huang, Z. Zheng, Y. Wu, M. Gao, Z. Su, and Y. Huang, ‘14-3-3 Proteins are Potential Regulators of Liquid–Liquid Phase Separation’, *Cell Biochem Biophys*, vol. 80, no. 2, pp. 277–293, June 2022, doi: 10.1007/s12013-022-01067-3.

[18] J. Hochmair *et al.*, ‘Stoichiometric 14-3-3ζ binding promotes phospho-Tau microtubule dissociation and reduces aggregation and condensation’, *Commun Biol*, vol. 8, no. 1, p. 1139,

July 2025, doi: 10.1038/s42003-025-08548-0.
[19] M. Falcicchio, J. A. Ward, S. Macip, and R. G. Doveston, 'Regulation of p53 by the 14-3-3 protein interaction network: new opportunities for drug discovery in cancer', *Cell Death Discov.*, vol. 6, no. 1, p. 126, Nov. 2020, doi: 10.1038/s41420-020-00362-3.
[20] K. V. Tugaeva *et al.*, 'The Mechanism of SARS-CoV-2 Nucleocapsid Protein Recognition by the Human 14-3-3 Proteins', *Journal of Molecular Biology*, vol. 433, no. 8, p. 166875, Apr. 2021, doi: 10.1016/j.jmb.2021.166875.
[21] E. C. Petronilho *et al.*, 'Phase separation of p53 precedes aggregation and is affected by oncogenic mutations and ligands', *Chem. Sci.*, vol. 12, no. 21, pp. 7334–7349, 2021, doi: 10.1039/D1SC01739J.
[22] T. M. Perdikari, A. C. Murthy, V. H. Ryan, S. Watters, M. T. Naik, and N. L. Fawzi, 'SARS‐CoV‐2 nucleocapsid protein phase‐separates with RNA and with human hnRNPs', *The EMBO Journal*, vol. 39, no. 24, p. e106478, Dec. 2020, doi: 10.15252/embj.2020106478.
[23] D. Šulskis, M. Žiaunys, A. Sakalauskas, R. Sniečkutė, and V. Smirnovas, 'Formation of amyloid fibrils by the regulatory 14-3-3 ζ protein', *Open Biol.*, vol. 14, no. 1, p. 230285, Jan. 2024, doi: 10.1098/rsob.230285.
[24] A. Aitken *et al.*, '14-3-3 proteins: a highly conserved, widespread family of eukaryotic proteins', *Trends in Biochemical Sciences*, vol. 17, no. 12, pp. 498–501, Dec. 1992, doi: 10.1016/0968-0004(92)90339-B.
[25] S. Ahmad *et al.*, 'The UniProt website API: facilitating programmatic access to protein knowledge', *Nucleic Acids Res*, vol. 53, no. W1, pp. W547–W553, July 2025, doi: 10.1093/nar/gkaf394.
[26] R. C. Edgar, 'MUSCLE: multiple sequence alignment with high accuracy and high throughput', *Nucleic Acids Res*, vol. 32, no. 5, pp. 1792–1797, Mar. 2004, doi: 10.1093/nar/gkh340.
[27] A. M. Waterhouse, J. B. Procter, D. M. A. Martin, M. Clamp, and G. J. Barton, 'Jalview Version 2—a multiple sequence alignment editor and analysis workbench', *Bioinformatics*, vol. 25, no. 9, pp. 1189–1191, May 2009, doi: 10.1093/bioinformatics/btp033.
[28] F. W. Studier, 'Protein production by auto-induction in high-density shaking cultures', *Protein Expression and Purification*, vol. 41, no. 1, pp. 207–234, May 2005, doi: 10.1016/j.pep.2005.01.016.
[29] K. Mikalauskaite, M. Ziaunys, T. Sneideris, and V. Smirnovas, 'Effect of Ionic Strength on Thioflavin-T Affinity to Amyloid Fibrils and Its Fluorescence Intensity', *IJMS*, vol. 21, no. 23, p. 8916, Nov. 2020, doi: 10.3390/ijms21238916.
[30] K. Mikalauskaite, M. Ziaunys, and V. Smirnovas, 'Lysozyme Amyloid Fibril Structural Variability Dependence on Initial Protein Folding State', *IJMS*, vol. 23, no. 10, p. 5421, May 2022, doi: 10.3390/ijms23105421.
[31] M. Ziaunys, D. Sulskis, D. Veiveris, A. Sakalauskas, K. Mikalauskaite, and V. Smirnovas, 'Diverse effects of fluorescent labels on alpha-synuclein condensate formation during liquid-liquid phase separation', *International Journal of Biological Macromolecules*, vol. 283, p. 137688, Dec. 2024, doi: 10.1016/j.ijbiomac.2024.137688.
[32] J. Schindelin *et al.*, 'Fiji: an open-source platform for biological-image analysis', *Nat Methods*, vol. 9, no. 7, pp. 676–682, July 2012, doi: 10.1038/nmeth.2019.
[33] S. Rajagopalan, R. S. Sade, F. M. Townsley, and A. R. Fersht, 'Mechanistic differences in the transcriptional activation of p53 by 14-3-3 isoforms', *Nucleic Acids Research*, vol. 38, no. 3, pp. 893–906, Jan. 2010, doi: 10.1093/nar/gkp1041.
[34] N. Louros, K. Konstantoulea, M. De Vleeschouwer, M. Ramakers, J. Schymkowitz, and F. Rousseau, 'WALTZ-DB 2.0: an updated database containing structural information of experimentally determined amyloid-forming peptides', *Nucleic Acids Research*, vol. 48, no. D1, pp. D389–D393, Jan. 2020, doi: 10.1093/nar/gkz758.
[35] J. Sun *et al.*, 'Precise prediction of phase-separation key residues by machine learning', *Nat Commun*, vol. 15, no. 1, p. 2662, Mar. 2024, doi: 10.1038/s41467-024-46901-9.

[36] V. Kotov *et al.*, ‘In-depth interrogation of protein thermal unfolding data with MoltenProt’, *Protein Sci*, vol. 30, no. 1, pp. 201–217, Jan. 2021, doi: 10.1002/pro.3986.
[37] M. Biancalana and S. Koide, ‘Molecular mechanism of Thioflavin-T binding to amyloid fibrils’, *Biochimica et Biophysica Acta - Proteins and Proteomics*, vol. 1804, no. 7, pp. 1405–1412, July 2010, doi: 10.1016/j.bbapap.2010.04.001.
[38] A. Barth, ‘Infrared spectroscopy of proteins’, *Biochimica et Biophysica Acta (BBA) - Bioenergetics*, vol. 1767, no. 9, pp. 1073–1101, Sept. 2007, doi: 10.1016/j.bbabio.2007.06.004.
[39] V. Foderà *et al.*, ‘Thioflavin T hydroxylation at basic pH and its effect on amyloid fibril detection.’, *The journal of physical chemistry. B*, vol. 112, no. 47, pp. 15174–81, Nov. 2008, doi: 10.1021/jp805560c.
[40] I. Baronaitė, D. Šulskis, A. Kopūstas, M. Tutkus, and V. Smirnovas, ‘Formation of Calprotectin Inhibits Amyloid Aggregation of S100A8 and S100A9 Proteins’, *ACS Chem. Neurosci.*, vol. 15, no. 9, pp. 1915–1925, May 2024, doi: 10.1021/acschemneuro.4c00093.
[41] J. Singh, A. T. Sabareesan, M. K. Mathew, and J. B. Udgaonkar, ‘Development of the Structural Core and of Conformational Heterogeneity during the Conversion of Oligomers of the Mouse Prion Protein to Worm-like Amyloid Fibrils’, *Journal of Molecular Biology*, vol. 423, no. 2, pp. 217–231, Oct. 2012, doi: 10.1016/j.jmb.2012.06.040.
[42] M. Pillai and S. K. Jha, ‘Early Metastable Assembly during the Stress-Induced Formation of Worm-like Amyloid Fibrils of Nucleic Acid Binding Domains of TDP-43’, *Biochemistry*, vol. 59, no. 3, pp. 315–328, Jan. 2020, doi: 10.1021/acs.biochem.9b00780.
[43] W. M. Babinchak and W. K. Surewicz, ‘Liquid–Liquid Phase Separation and Its Mechanistic Role in Pathological Protein Aggregation’, *Journal of Molecular Biology*, vol. 432, no. 7, pp. 1910–1925, Mar. 2020, doi: 10.1016/j.jmb.2020.03.004.
[44] K. Dörner *et al.*, ‘Fluorescent protein and peptide tags alter condensate formation and dynamics in vivo and in vitro’, *EMBO Rep*, Nov. 2025, doi: 10.1038/s44319-025-00626-y.
[45] T. Mittag and R. Parker, ‘Multiple Modes of Protein–Protein Interactions Promote RNP Granule Assembly’, *Journal of Molecular Biology*, vol. 430, no. 23, pp. 4636–4649, Nov. 2018, doi: 10.1016/j.jmb.2018.08.005.
[46] Y.-Q. Liu *et al.*, ‘14-3-3ζ Participates in the Phase Separation of Phosphorylated and Glycated Tau and Modulates the Physiological and Pathological Functions of Tau’, *ACS Chem. Neurosci.*, vol. 14, no. 7, pp. 1220–1225, Apr. 2023, doi: 10.1021/acschemneuro.3c00034.
[47] J. Fehilly *et al.*, ‘Condensate formation of the human RNA-binding protein SMAUG1 is controlled by its intrinsically disordered regions and interactions with 14-3-3 proteins’, Feb. 10, 2023, *Molecular Biology*. doi: 10.1101/2023.02.09.527857.
[48] A. R. Strom and C. P. Brangwynne, ‘The liquid nucleome – phase transitions in the nucleus at a glance’, *Journal of Cell Science*, vol. 132, no. 22, p. jcs235093, Nov. 2019, doi: 10.1242/jcs.235093.
[49] T. Umahara, T. Uchihara, K. Tsuchiya, A. Nakamura, and T. Iwamoto, ‘Intranuclear localization and isoform-dependent translocation of 14-3-3 proteins in human brain with infarction’, *Journal of the Neurological Sciences*, vol. 260, no. 1–2, pp. 159–166, Sept. 2007, doi: 10.1016/j.jns.2007.04.053.
[50] A. Brunet *et al.*, ‘14-3-3 transits to the nucleus and participates in dynamic nucleocytoplasmic transport’, *The Journal of Cell Biology*, vol. 156, no. 5, pp. 817–828, Mar. 2002, doi: 10.1083/jcb.200112059.
[51] M. Liu *et al.*, ‘Proteins Associated with Cognition in Amyloid-beta Positive Elders Based on Cerebrospinal Fluid Proteomics’, *Mol Neurobiol*, vol. 63, no. 1, p. 327, Jan. 2026, doi: 10.1007/s12035-025-05442-y.
[52] M. Ikeda *et al.*, ‘Identification of YWHAE, a gene encoding 14-3-3epsilon, as a possible susceptibility gene for schizophrenia’, *Human Molecular Genetics*, vol. 17, no. 20, pp. 3212–3222, Oct. 2008, doi: 10.1093/hmg/ddn217.
[53] K. Toyo-oka *et al.*, ‘14-3-3ε is important for neuronal migration by binding to NUDEL: a

molecular explanation for Miller–Dieker syndrome', *Nat Genet*, vol. 34, no. 3, pp. 274–285, July 2003, doi: 10.1038/ng1169.

[54] J.-H. Park *et al.*, 'Amyotrophic lateral sclerosis-related mutant superoxide dismutase 1 aggregates inhibit 14-3-3-mediated cell survival by sequestration into the JUNQ compartment', *Human Molecular Genetics*, vol. 26, no. 18, pp. 3615–3629, Sept. 2017, doi: 10.1093/hmg/ddx250.

[55] G. Di Fede *et al.*, 'The ε Isoform of 14-3-3 Protein Is a Component of the Prion Protein Amyloid Deposits of Gerstmann-Sträussler-Scheinker Disease':, *Journal of Neuropathology and Experimental Neurology*, vol. 66, no. 2, pp. 124–130, Feb. 2007, doi: 10.1097/nen.0b013e3180302060.

[56] Z. Xu *et al.*, '14-3-3 targets chaperone-associated misfolded proteins to aggresomes', *Journal of Cell Science*, p. jcs.126102, Jan. 2013, doi: 10.1242/jcs.126102.

[57] M. Yano, S. Nakamuta, X. Wu, Y. Okumura, and H. Kido, 'A Novel Function of 14-3-3 Protein: 14-3-3ζ Is a Heat-Shock–related Molecular Chaperone That Dissolves Thermal-aggregated Proteins', *Molecular Biology of the Cell*, vol. 17, no. 11, pp. 4769–4779, Nov. 2006, doi: 10.1091/mbc.e06-03-0229.

[58] N. N. Sluchanko and N. B. Gusev, 'Moonlighting chaperone-like activity of the universal regulatory 14-3-3 proteins', *FEBS Journal*, vol. 284, no. 9, pp. 1279–1295, 2017, doi: 10.1111/febs.13986.